VIP Nanocrystals

DOI: 10.1002/ange.201107061

Controlling the Nucleation and Growth of Silver on Palladium Nanocubes by Manipulating the Reaction Kinetics**

*Jie Zeng, Cun Zhu, Jing Tao, Mingshang Jin, Hui Zhang, Zhi-Yuan Li, Yimei Zhu, and Younan Xia**

Bimetallic nanocrystals are often advantageous over single-component systems for a range of fundamental studies and applications because the associated variations in compositions and spatial distributions provide additional handles for experimentally maneuvering both the structures and properties.[1–3] For example, a bimetallic system may exhibit either localized surface plasmon resonance (LSPR) or catalytic properties different from each one of the constituent metals depending on the electronic coupling between the two metals.[4–9] Up till now, a number of noble metals, such as Au, Ag, Pd, Pt, and Rh have been combined to generate bimetallic nanocrystals with tunable and enhanced properties.[1–8,10–13] With regard to the spatial distributions of elements in a bimetallic system, three patterns have been observed and exploited: 1) homogeneously distributed as in an alloy or intermetallic compound;[5,6] 2) separated into two concentric layers as in a core-shell structure;[2,7,10–12] and 3) separated into two side-by-side regions as in a dimeric structure.[3,8,12]

Seed-mediated growth is probably the most powerful route to bimetallic nanocrystals, where pre-formed seeds of one metal serve as the sites of nucleation and then growth for another metal. It has been observed that the nucleation and growth mode of the second metal are governed by a number of physical parameters, including the (mis)match of lattice structures and constants, the correlation of surface and interface energies, and difference in electronegativity between the two metals.[5,11] For two given metals, these parameters would direct the heterogeneous nucleation and growth on a seed to follow a conformal or site-selective mode, generating a core–shell or hybrid structure. Although a recent study from our group demonstrates that these two types of bimetallic structures can both be produced with good yields in the Pd–Au system by judicially choosing a reducing agent,[12] it remains a grand challenge to spatially control the sites involved in nucleation, especially for nanocrystal seeds enclosed by a set of equivalent faces.

We suspect that the nucleation and growth of a nanocrystal seed is highly sensitive to the rate at which the atoms to be deposited are generated from a precursor. This rate can be manipulated using at least three different strategies: 1) variation of the reductant and/or precursor; 2) tuning of the reaction temperature; and 3) control of precursor concentration. The last approach should be most attractive in terms of simplicity and versatility. To this end, we recently demonstrated the use of a syringe pump as an effective means to manipulate the precursor concentration and thus selectively enhance the overgrowth of Rh along the corners and edges rather than side faces of a cubic seed.[13] Herein, we further extend the capability of this approach to achieve nucleation and growth of Ag on one, three, and six of the equivalent {100} faces on a Pd seed. By simply manipulating the rate at which $AgNO_3$ was added, we found that Pd–Ag bimetallic nanocrystals with three distinct structures could be produced under otherwise similar conditions: dimers with Ag growing on only one of the six faces of a Pd seed; eccentric hybrid bars with Ag growing on three adjacent faces of a Pd seed; and core–shell nanocrystals with Ag growing on all six faces of a Pd seed. Significantly, these Pd–Ag bimetallic nanocrystals displayed substantially different LSPR properties as compared with those made of pure Pd, Ag, or their alloys.

In the first step, we synthesized Pd seeds by reducing Na_2PdCl_4 with L-ascorbic acid (AA) in an aqueous solution in the presence of bromide ions as a capping agent to promote the formation of {100} facets.[14] A transmission electron microscopy (TEM) image of the as-prepared Pd seeds is shown in Figure S1 in the Supporting Information. The nanocrystals had an average edge length of 18 nm, together with an average aspect ratio of 1:1.2. Each one of them was enclosed by six {100} facets: two of them were square in shape (type-*a*) while the other four were slightly rectangular (type-*b*). These nanocrystals then served as seeds for the overgrowth of Ag in the next step.

[*] Dr. J. Zeng, C. Zhu, M. Jin, Dr. H. Zhang, Prof. Y. Xia
Department of Biomedical Engineering, Washington University
St. Louis, MO 63130 (USA)
E-mail: xia@biomed.wustl.edu
Dr. J. Tao, Dr. Y. Zhu
Condensed Matter Physics & Materials Science Department
Brookhaven National Laboratory, Upton, NY 11973 (USA)
Dr. Z.-Y. Li
Institute of Physics, Chinese Academy of Sciences
Beijing 100080 (P. R. China)

[**] This work was supported in part by grants from the NSF (DMR, 0804088 and 1104616) and startup funds from Washington University in St. Louis. Y.X. was also partially supported by the World Class University (WCU) program through the National Research Foundation of Korea funded by the Ministry of Education, Science and Technology (R32-20031). Part of the research was performed at the Nano Research Facility (NRF), a member of the National Nanotechnology Infrastructure Network (NNIN), which is funded by the NSF under award no. ECS-0335765. The work at BNL was supported by the U.S. Department of Energy, Basic Energy Sciences, by the Materials Sciences and Engineering Division under Contract No. DE-AC02-98CH10886 and through the use of CFN.

Supporting information for this article is available on the WWW under http://dx.doi.org/10.1002/anie.201107061.

We conducted the seeded growth of Ag on Pd by introducing an aqueous $AgNO_3$ solution into an aqueous mixture containing both the Pd seeds and ascorbic acid (AA) at a well-defined, adjustable rate. Figure 1 a–c, shows typical TEM images of the products obtained after different volumes of the $AgNO_3$ solution had been added at a rate of 1.0 mL h^{-1}. At this injection rate, Ag atoms only nucleated and grew on one of the six faces of a Pd seed, generating a Pd–Ag bimetallic dimer with a hybrid structure. In the early stage, the Ag was deposited as a thin plate on one of the six faces of a seed. Further growth resulted in the formation of a Ag plate, cube, and then bar with slight truncations at the corners. During the growth process, the lateral dimensions of the Ag block also increased slightly. Statistical analysis indicates that the Ag atoms preferentially nucleated and grew on the type-*b* face for most (> 80 %) of the Pd seeds. When the injection rate for $AgNO_3$ solution was increased to 30 mL h^{-1}, a different morphology was observed for the final products (Figure 1 d–f). At this rate, Ag atoms were able to nucleate and grow on as many as three adjacent faces of a Pd seed. When a small amount (0.5 mL, Figure 1 d) of $AgNO_3$ was introduced, the Ag atoms were mainly deposited on one of the six faces of a Pd seed, similar to what was observed in Figure 1 a.

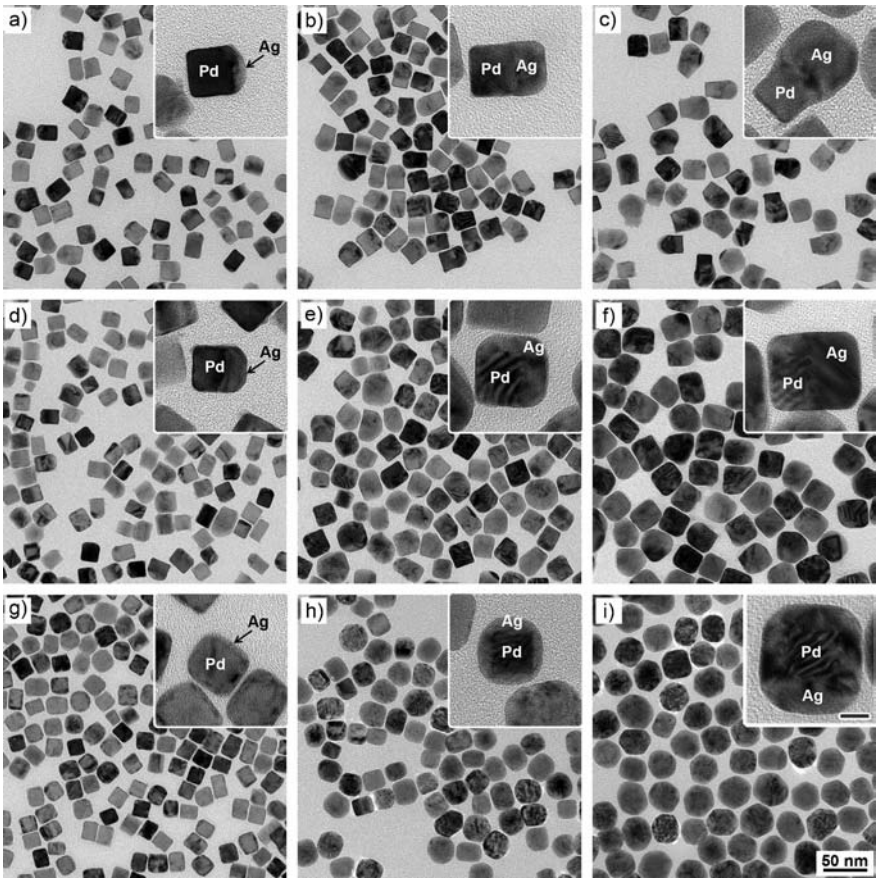

Figure 1. Synthesis of three different types of Pd–Ag bimetallic nanocrystals by controlling the injection rate of $AgNO_3$. a–c) TEM images of Pd–Ag dimers obtained by injecting the $AgNO_3$ solution at 1 mL h^{-1}, the total volumes of added $AgNO_3$ solution were: a) 0.4, b) 1.5, and c) 2.7 mL. d–f) TEM images of Pd–Ag eccentric nanobars obtained by injecting the $AgNO_3$ solution at 30 mL h^{-1}, the total volumes of added $AgNO_3$ solution were: d) 0.5, e) 1.7, and f) 3.3 mL. g–i) TEM images of Pd@Ag core–shell nanocrystals obtained by adding all of the $AgNO_3$ solution at one time, the total volumes of added $AgNO_3$ solution were: g) 0.5, h) 1.7, and i) 3.3 mL. Insets: enlargements, scale 10 nm and applies to all insets. The 50 nm scale bar applies to all main images.

As the amount of $AgNO_3$ solution was increased to 1.7 mL (Figure 1 e), however, the Ag atoms were able to grow from three adjacent faces of a Pd seed, producing a Pd–Ag eccentric nanobar with the Pd seed positioned at one of the corners. Specifically, the Ag atoms were added to one of the type-*a* faces and two adjacent type-*b* faces of the Pd seed. A careful analysis indicates that the Ag grew slightly faster along the direction perpendicular to the type-*b* face than that to the type-*a* face. Significantly, the site selectivity of this overgrowth mode could be retained when more $AgNO_3$ was introduced (Figure 1 f). Owing to the superposition of two slightly misfit crystalline lattices associated with Pd and Ag, we could easily observe a Moiré pattern where the region corresponding to the Pd seed was covered by fringes with alternative bright and dark stripes.[15] For the products in Figure 1 e,f, the Moiré patterns could be easily observed since either the top or the bottom face of the Pd seed was covered by Ag (see Supporting Information, Figure S2 for images at a higher magnification). The Moiré fringes in the Pd region suggest that the (200) lattice fringes of Ag and Pd were aligned parallel to each other and there was an epitaxial relationship between the Ag and Pd components.

As expected, when the $AgNO_3$ solution was quickly injected into the reaction using a pipette, we observed nucleation and overgrowth of Ag on the entire surface of a Pd seed, resulting in the formation of a Pd@Ag core–shell nanocrystal (Figure 1 g–i). When the amount of $AgNO_3$ solution was relatively small (Figure 1 g), the Ag overlayer was still able to cover all six faces of a Pd seed although its thickness was only on the order of 1–2 nm. Increasing the amount of $AgNO_3$ solution merely increased the thickness of the Ag shell (Figure 1 h,i).

We characterized these three different types of Pd–Ag nanocrystals with high-resolution TEM (HRTEM), scanning TEM (STEM), and energy dispersive X-ray (EDX) microanalysis. All the HRTEM images (Figure 2 a, d, and g) indicate that the lattice fringes were coherently extended from the Pd core to the Ag region, suggesting an epitaxial relationship between these two metals. The {200} fringes in

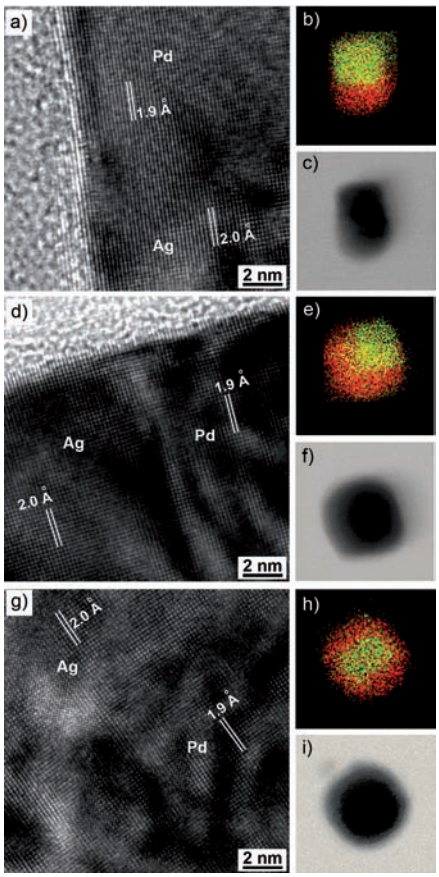

Figure 2. Structural analyses of the three different types of Pd–Ag bimetallic nanocrystals. a),d),g) HRTEM images, b),e),h) EDX mapping images, and c),f),i) bright-field STEM images of the individual nanocrystals shown in Figure 1 (b), (e), and (h), respectively. For EDX mapping, Pd atoms are shown in green and Ag atoms are shown in orange.

the Pd and Ag regions showed periods of 1.9 and 2.0 Å, as expected for face-centered cubic (fcc) Pd and Ag, respectively. Although the lattice constants of Pd and Ag have a mismatch of 4.5%, the Ag atoms could still nucleate and epitaxially grow from the {100} facets of a Pd seed possibly due to the small size of the seed. The HRTEM images showed only a very minor difference in contrast between the Pd and Ag regions due to their similar atomic numbers.[16] The distributions of Pd and Ag were clearly resolved by EDX spectra (Supporting Information, Figure S3), EDX elemental mapping (Figure 2b, e, and h and Supporting Information, Figure S4), and the corresponding bright-field STEM images (Figure 2c, f, and i). All the data support the formation of three distinctive types of structures as we have described in the prior section. The selected area electron diffraction (SAED) patterns (insets of Supporting Information, Figure S5–S7) recorded from the relevant particles also show a single-crystal nature for both Pd and Ag components.

Figure 3 schematically illustrates the three distinct modes observed for the overgrowth of Ag on Pd seeds when $AgNO_3$ was introduced at different rates. In general, when $AgNO_3$ is introduced into an aqueous solution containing AA and the Pd seeds, this salt precursor is immediately reduced to Ag

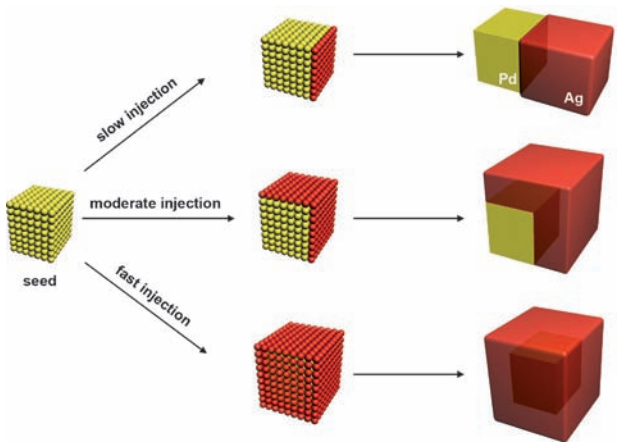

Figure 3. Three different mechanisms for the nucleation and growth of Ag on Pd seeds as controlled by the rate of injection. The reaction rate increases from top to bottom.

atoms upon contact with AA.[17] As such, the reduction rate and thus the concentration of Ag atoms are mainly determined by the injection rate used for introducing the $AgNO_3$ solution. At a slow injection rate, the concentration of Ag atoms derived from $AgNO_3$ can be maintained at a relatively low level around the Pd seed. The Ag atoms will preferentially nucleate on the surface of a Pd seed via heterogeneous nucleation rather than in the solution phase by themselves via homogeneous nucleation due to a lower activation energy for the former pathway.[18] When the concentration is too low, the Ag atoms cannot generate multiple nucleation sites on a Pd seed. Instead, only one of the six faces of a Pd seed is involved in the heterogeneous nucleation. Due to the self-catalytic behavior of Ag, once a nucleus of Ag atoms has been created on the surface of a seed, the reduction of $AgNO_3$ in the following step will preferentially occur at this site rather than other regions on the Pd seed. The Ag nucleus initially grows laterally across the face of a Pd seed and then vertically along the direction perpendicular to the face, evolving into a plate, cube, and then bar. The reason why the Ag atoms preferentially nucleate on the type-*b* rather than type-*a* face of a Pd seed can be attributed to their difference in actual surface areas and thus different collision frequencies with the Ag atoms.

When the injection rate is very fast, the Ag atoms around a Pd seed can be maintained at a level sufficiently high to facilitate nucleation on all faces of a Pd seed, leading to the formation of a conformal Ag shell. A similar mechanism is also involved when $AgNO_3$ is injected at a moderate rate and the concentration of Ag atoms is only high enough to allow nucleation on three of the six faces of a Pd seed. In the very early stage, however, the amount of added $AgNO_3$ may just be sufficient for nucleation and growth on one of the six faces of a Pd seed (Figure 1d). Further addition of $AgNO_3$ then leads to nucleation on two adjacent faces, ultimately forming Pd–Ag eccentric nanocrystals with the Pd seed located at one of the corners. The reason why Ag preferred to deposit on three adjacent faces instead of all type-*b* faces might be related to the migration of Ag atoms on a Pd seed.[19]

Specifically, the initially deposited Ag atoms may migrate to adjacent faces and then serve as catalytic centers for further growth of Ag.

Figure 4 shows the extinction spectra recorded from aqueous suspensions of the as-prepared Pd–Ag bimetallic nanocrystals. In comparison, the extinction spectrum of the

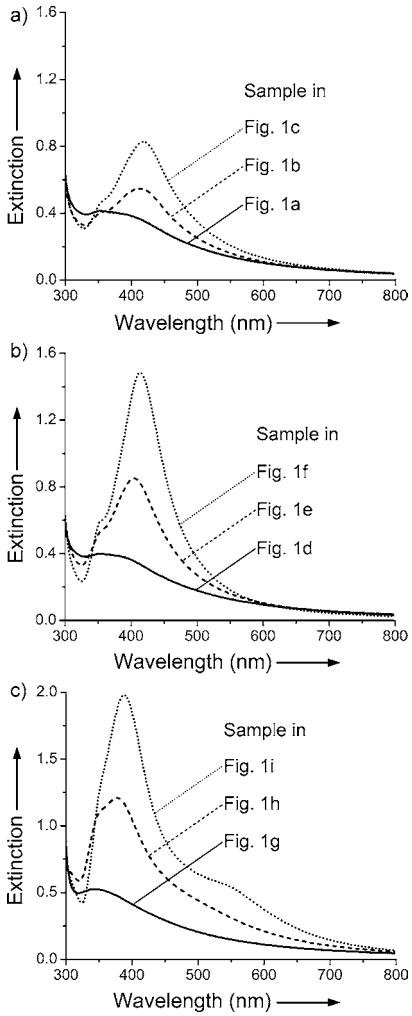

Figure 4. UV/Vis extinction spectra of the three different types of Pd–Ag bimetallic nanocrystals: a) the Pd–Ag dimers where the bottom, middle, and top traces correspond to the samples shown in Figure 1 a,b,c, respectively; b) the Pd–Ag eccentric nanobars where the bottom, middle, and top traces correspond to samples shown in Figure 1 d,e,f, respectively; and c) the Pd@Ag core–shell nanocrystals where the bottom, middle, and top traces correspond to samples shown in Figure 1 g,h,i, respectively.

Pd seeds (Supporting Information, Figure S8) shows no LSPR peak in the visible region. For the Pd–Ag dimeric nanocrystals, the major LSPR peak associated with the Ag portion was observed in the range of 420–425 nm, accompanied by a shoulder peak around 350 nm (Figure 4 a). The peak positions were slightly red-shifted as the deposited Ag evolved from thin plates into bars, reflecting the size sensitivity for the LSPR peak of Ag nanostructures. Similar red-shifts were also observed for the samples obtained under two other growth modes. For the Pd–Ag eccentric nanobars (Figure 4 b), the peak positions were similar to those of Pd–Ag dimers, but the peak intensities were much stronger. For the Pd@Ag core–shell samples, the major LSPR peak appeared at relatively shorter wavelengths (380–395 nm Figure 4 c), overlapping with a shoulder peak at approximately 350 nm. Interestingly, a weak peak arose at 550 nm during the growth of Ag shells, most likely due to the elongation associated with the Ag shells. Compared with the other two cases, the major LSPR peaks for the core-shell nanocrystals were the strongest and sharpest.

These results were consistent with the trend observed in theoretical calculations where the extinction spectra (Supporting Information, Figure S9, b–d) of three typical Pd–Ag bimetallic nanocrystals were computed using the discrete dipole approximation (DDA) method.[20] A comparison with the DDA spectra revealed that no peak appeared around 350 nm for both solid and hollow Ag nanostructures with the same outer diameter (Figure S10).[21] On the contrary, this peak appeared for a Pd cube with a 8 nm layer of Ag on one of the six faces (Figure S9a). Thus, the Pd–Ag interface must be responsible for this shoulder peak. The major LSPR of a Pd@Ag core–shell nanocrystal also occurred at a shorter wavelength than those of the solid and hollow nanostructures made of pure Ag (Figure S10), clearly indicating that the LSPR was blue-shifted as a result of the incorporation of a Pd core. This phenomenon can be attributed to the increase in surface electron density in the Ag shell, as driven by electron transfer from Pd to Ag because of a higher electron chemical potential for Pd relative to Ag.[22]

In summary, we have demonstrated that we could achieve nucleation and growth of Ag on one, three, or six of the equivalent {100} faces of a Pd seed by simply controlling the rate at which the precursor was introduced and reduced. As such, we obtained bimetallic nanocrystals with three distinctive structures under otherwise similar experimental conditions: hybrid dimers, eccentric nanobars, and core–shell nanocrystals. These bimetallic nanocrystals are attractive for applications in photonics as they displayed different LSPR properties as compared with those consisting of pure metals and their alloys. This strategy for engineering the spatial distributions of elements in a bimetallic nanocrystal offers a radically different approach to the fabrication of plasmonic nanostructures with enhanced sensing and SERS capabilities.

Received: October 6, 2011
Published online: November 21, 2011

Keywords: nanocrystals · palladium · seed-mediated growth · silver · surface plasmon resonance

[1] a) P. D. Cozzoli, T. Pellegrino, L. Manna, *Chem. Soc. Rev.* **2006**, *35*, 1195; b) B. Lim, M. Jiang, P. H. C. Camargo, E. C. Cho, J. Tao, X. Lu, Y. Zhu, Y. Xia, *Science* **2009**, *324*, 1302.

[2] a) B. Rodríguez-González, A. Burrows, M. Watanabe, C. J. Kiely, L. M. Liz-Marzán, *J. Mater. Chem.* **2005**, *15*, 1755; b) S. E. Habas, H. Lee, V. Radmilovic, G. A. Somorjai, P. Yang, *Nat. Mater.* **2007**, *6*, 692; c) F. Tao, M. E. Grass, Y.

Zhang, D. R. Butcher, J. R. Renzas, Z. Liu, J. Y. Chung, B. S. Mun, M. Salmeron, G. A. Somorjai, *Science* **2008**, *322*, 932.
[3] a) H. Lee, S. E. Habas, G. A. Somorjai, P. Yang, *J. Am. Chem. Soc.* **2008**, *130*, 5406; b) D. Seo, C. I. Yoo, J. Jung, H. Song, *J. Am. Chem. Soc.* **2008**, *130*, 2940; c) R. Costi, A. E. Saunders, U. Banin, *Angew. Chem.* **2010**, *122*, 4996; *Angew. Chem. Int. Ed.* **2010**, *49*, 4878; d) M. R. Langille, J. Zhang, C. A. Mirkin, *Angew. Chem.* **2011**, *123*, 3605; *Angew. Chem. Int. Ed.* **2011**, *50*, 3543.
[4] S. Zhou, K. McIlwrath, G. Jackson, B. Eichhorn, *J. Am. Chem. Soc.* **2006**, *128*, 1780.
[5] Z. Peng, H. Yang, *Nano Today* **2009**, *4*, 143.
[6] a) V. R. Stamenkovic, B. Fowler, B. S. Mun, G. Wang, P. N. Ross, C. A. Lucas, N. M. Marković, *Science* **2007**, *315*, 493; b) J. Zhang, H. Yang, J. Fang, S. Zou, *Nano Lett.* **2010**, *10*, 638.
[7] a) D. Xu, Z. Liu, H. Yang, Q. Liu, J. Zhang, J. Fang, S. Zou, K. Sun, *Angew. Chem.* **2009**, *121*, 4281; *Angew. Chem. Int. Ed.* **2009**, *48*, 4217; b) Z. Peng, H. Yang, *J. Am. Chem. Soc.* **2009**, *131*, 7542; c) C. Wang, D. Van Der Vliet, K. L. More, N. J. Zaluzec, S. Peng, S. Sun, H. Daimon, G. Wang, J. Greeley, J. Pearson, A. P. Paulikas, G. Karapetrov, D. Strmcnik, N. M. Markovic, V. R. Stamenkovic, *Nano Lett.* **2011**, *11*, 919; d) K. Tedsree, T. Li, S. Jones, C. W. A. Chan, K. M. K. Yu, P. A. J. Bagot, E. A. Marquis, G. D. W. Smith, S. C. E. Tsang, *Nat. Nanotechnol.* **2011**, *6*, 302.
[8] J. Zhang, K. Sasaki, E. Sutter, R. R. Adzic, *Science* **2007**, *315*, 220.
[9] a) R. Elghanian, J. J. Storhoff, R. C. Mucic, R. L. Letsinger, C. A. Mirkin, *Science* **1997**, *277*, 1078; b) E. Hao, G. C. Schatz, *J. Chem. Phys.* **2004**, *120*, 357; c) C. Sönnichsen, B. M. Reinhard, J. Liphardt, A. P. Alivisatos, *Nat. Biotechnol.* **2005**, *23*, 741; d) J. Aizpurua, G. W. Bryant, L. J. Richter, F. J. G. de Abajo, *Phys. Rev. B* **2005**, *71*, 235420; e) K-S. Lee, M. A. El-Sayed, *J. Phys. Chem. B* **2006**, *110*, 19220; f) K. A. Willets, R. P. V. Duyne, *Annu. Rev. Phys. Chem.* **2007**, *58*, 267; g) M. K. Kinnan, G. Chumanov, *J. Phys. Chem. C* **2010**, *114*, 7496; h) M. A. Mahmoud, M. A. El-Sayed, *Nano Lett.* **2011**, *11*, 946.
[10] a) C. Xue, J. E. Millstone, S. Li, C. A. Mirkin, *Angew. Chem.* **2007**, *119*, 8588; *Angew. Chem. Int. Ed.* **2007**, *46*, 8436; b) H. Yoo, J. E. Millstone, S. Li, J.-W. Jang, W. Wei, J. Wu, G. C. Schatz, C. A. Mirkin, *Nano Lett.* **2009**, *9*, 3038; c) V. Mazumder, M. Chi, S. Sun, *Angew. Chem.* **2010**, *122*, 9558; *Angew. Chem. Int. Ed.* **2010**, *49*, 9368; d) F. Wang, C. Li, L.-D. Sun, H. Wu, T. Ming, J. Wang, J. C. Yu, C.-H. Yan, *J. Am. Chem. Soc.* **2011**, *133*, 1106; e) F. Wang, L.-D. Sun, W. Feng, H. Chen, M. H. Yeung, J. Wang, C.-H. Yan, *Small* **2010**, *6*, 2566.
[11] F.-R. Fan, D.-Y. Liu, Y.-F. Wu, S. Duan, Z.-X. Xie, Z.-Y. Jiang, Z.-Q. Tian, *J. Am. Chem. Soc.* **2008**, *130*, 6949.
[12] B. Lim, H. Kobayashi, T. Yu, J. Wang, M. J. Kim, Z-Y. Li, M. Rycenga, Y. Xia, *J. Am. Chem. Soc.* **2010**, *132*, 2506.
[13] H. Zhang, W. Li, M. Jin, J. Zeng, T. Yu, D. Yang, Y. Xia, *Nano Lett.* **2011**, *11*, 898.
[14] M. Jin, H. Liu, H. Zhang, Z. Xie, J. Liu, Y. Xia, *Nano Res.* **2011**, *4*, 83.
[15] D. B. Williams, C. B. Carter, *Transmission Electron Microscopy, a Text for Materials Science*, Plenum, New York, **1996**.
[16] Z. L. Wang, *J. Phys. Chem. B* **2000**, *104*, 1153.
[17] a) J. Zeng, Y. Zheng, M. Rycenga, J. Tao, Z-Y. Li, Q. Zhang, Y. Zhu, Y. Xia, *J. Am. Chem. Soc.* **2010**, *132*, 8552; b) Q. Zhang, Y. Hu, S. Guo, J. Goebl, Y. Yin, *Nano Lett.* **2010**, *10*, 5037.
[18] Y. Xia, Y. Xiong, B. Lim, S. E. Skrabalak, *Angew. Chem.* **2009**, *121*, 62; *Angew. Chem. Int. Ed.* **2009**, *48*, 60.
[19] a) Q. Zhang, J. Ge, T. Pham, J. Goebl, Y. Hu, Z. Lu, Y. Yin, *Angew. Chem.* **2009**, *121*, 3568; *Angew. Chem. Int. Ed.* **2009**, *48*, 3516; b) J. Zeng, S. Roberts, Y. Xia, *Chem. Eur. J.* **2010**, *16*, 12559.
[20] K. L. Kelly, E. Coronado, L. L. Zhao, G. C. Schatz, *J. Phys. Chem. B* **2003**, *107*, 668.
[21] J. B. Jackson, N. J. Halas, *J. Phys. Chem. B* **2001**, *105*, 2743.
[22] a) *CRC Handbook of Chemistry and Physics* 88th ed. (Ed.: D. R. Lide), CRC/Taylor and Francis, Boca Raton, **2008**; b) C. Novo, A. M. Funston, A. K. Gooding, P. Mulvaney, *J. Am. Chem. Soc.* **2009**, *131*, 14664; c) J. M. Luther, P. K. Jain, T. Ewers, A. P. Alivisatos, *Nat. Mater.* **2011**, *10*, 361.

